



Techno-economic assessment of evacuated flat-plate solar collector system for industrial process heat

Zohaib Hassan¹ | Mariam Mahmood¹ | Naveed Ahmed¹ |
 Muhammad H. Saeed¹ | Rashid Khan² | Muhammad Mujtaba Abbas³  |
 Md Abul Kalam⁴ | Fares Almomani⁵  | Emad Abdelsalam⁶

¹US-Pakistan Centre for Advanced Studies in Energy (USPCAS-E), National University of Science and Technology (NUST), Islamabad, Pakistan

²Atta-Ur-Rahman School of Applied Biosciences (ASAB), National University of Science and Technology (NUST), Islamabad, Pakistan

³Department of Mechanical Engineering, University of Engineering and Technology, Lahore, Pakistan

⁴School of Civil and Environmental Engineering, Faculty of Engineering and Information Technology, University of Technology Sydney, Ultimo, NSW, Australia

⁵Department of Chemical Engineering, Collage of Engineering, Qatar University, Doha, Qatar

⁶School of Engineering Technology, Al Hussein Technical University, Amman, Jordan

Correspondence

Fares Almomani, Department of Chemical Engineering, College of Engineering, Qatar University, P.O. Box: 2713, Doha, Qatar.
 Email: falmomani@qu.edu.qa

Abstract

In the industrial sector, hot water applications constitute a significant share of final energy consumption. This creates a wide demand-supply energy gap that must be bridged by integrating renewable sources with conventional fuels. This paper presents the performance analysis of a solar water heating system based on an evacuated flat-plate collector (EFPC) with a surface area of 4 m². A water-glycol mixture was used as the heat transfer fluid (HTF) with mass flow rates of 0.03, 0.0336, and 0.0504 kg/s under a vacuum pressure of −0.8 bar created inside the collector. A detailed numerical model was developed in MATLAB for the proposed EFPC system, followed by experimental validation. A maximum root mean square error of 2.81 for the absorber temperature and a percentage error of 6.62 was observed for the thermal efficiency in model validation. This substantiates the model's capability to predict actual system performance with reasonable accuracy. The maximum thermal efficiency of the EFPC is 78% with a maximum fluid outlet temperature of 98°C in June and 69°C in January. The maximum useful energy extracted is 1300 W in January. Additionally, the effect of design parameters on system performance such as mass flow rates, collector areas, tube spacing, and different HTF mixtures is simulated. Lastly, an economic analysis of the EFPC was conducted for hot water demand in a textile industry. The results revealed a payback period of 7.4 years, which highlights the feasibility of this system.

KEYWORDS

economic analysis, evacuated flat-plate collector, process heat, solar energy, thermal efficiency

1 | INTRODUCTION

Industrial production remains dependent upon fossil fuels, which are the main source of greenhouse gas (GHG) emissions worldwide.^{1,2} Industrial sectors consume approximately 35% of the total global energy,

which is comprised of about 30% for low-temperature applications, 22% for intermediate-temperature ranges, and 48% for higher thermal outputs. Additionally, the high concentration of GHG has increased global warming at alarming rates, particularly in developing countries.³ According to United Nations estimates, global

This is an open access article under the terms of the Creative Commons Attribution License, which permits use, distribution and reproduction in any medium, provided the original work is properly cited.

© 2023 The Authors. *Energy Science & Engineering* published by Society of Chemical Industry and John Wiley & Sons Ltd.

warming will reach 2°C above preindustrial levels, unless strict measures are taken to reduce GHG emissions.^{4,5} Developing countries face energy scarcity as they are primarily dependent upon fossil fuels.⁶ In developing countries like Pakistan, the total power generation in 2017 was approximately 23,718 MW and energy consumption has increased by 80% in the last 15 years, and this was expected to reach 40,000 MW by 2020.⁷ However, the total power generation capacity of Pakistan in 2021 was 37261 MW, which has increased by 11.5% to 41,557 MW in 2022, but still a deficit of 9000 MW when the demand peaks.⁸

Over the past two decades, fossil fuels have largely failed to resolve the persistent energy crisis in Pakistan.⁹ As such, the global consensus to mitigate environmental pollutants through the adoption of clean energy has necessitated the commercialization of clean, inexpensive, and efficient renewable sources for industrial applications in developing countries.¹⁰ For instance, solar energy has emerged as the best choice for meeting rising energy demands due to its wide abundance, ease of hybridization, and cost-effectiveness. Solar thermal applications include hot water systems, air heating, and combined heat and power generation.^{11–14} In developing countries, the textile industry—especially with the production of cotton—significantly impacts their total exports. Moreover, within the textile industry, conventional boilers fed by natural gas or electricity are used for hot water and steam generation.¹⁵ With the exception of an acute energy crisis, solar water heating systems are a promising and sustainable substitute for conventional fuels and have been introduced for domestic heating applications. Moreover, there is a greater potential for solar energy on an industrial and commercial scale in developing countries particularly.¹⁶

For nonconcentrating thermal collectors, there are flat-plate collectors (FPCs), evacuated tube collectors (ETCs), and evacuated flat-plate collectors (EFPCs). The EFPCs consist of a glazing glass fixed at the top of the collector, an absorber plate that absorbs solar energy and converts it into heat, and an array of fins attached between the collector plate and the glass cover to protect it from vacuum-induced high air pressure load. Working fluid circulates inside the closed heating loop that absorbs heat from the plate and transfers it to the secondary fluid in the heat exchanger. Gao et al.¹⁷ developed a numerical model for EFPCs in MATLAB, followed by a structural design of a medium-scale EFPC system and its experimental validation for medium-temperature application. Two types of EFPCs with different enclosure designs were also examined by developing a numerical model followed by a prototype tested under a solar simulator.¹⁸ The researchers discussed the overall temperatures, efficiencies, and reduction of losses with a vacuum.¹⁸

The EFPC model is validated through simulation and compared to other solar alternatives such as photovoltaic panels, photovoltaic thermal panels, FPCs, and ETCs to examine operational effectiveness.¹⁹ EFPCs have been investigated for domestic and commercial applications, but there is a research gap in its design optimization and economic analysis for industrial process heat applications. Figure 1 illustrates a cross-section view of the EFPC model. By creating a vacuum inside the collector enclosure, thermal losses are reduced, which results in temperatures greater than 100°C and higher efficiencies.²⁰

The evacuated enclosure creates insulation between the top and back cover and minimizes the heat loss from the absorber, which enables the EFPCs to replace conventional insulation.²¹ The EFPCs can achieve higher thermal outputs due to the vacuum generated between the absorber and the glass cover. These collectors are also efficient in low irradiance. Hassan et al.²² highlighted the usefulness of the EFPCs through comparison with a simple FPC. The model results demonstrated how the EFPC coefficients of thermal losses were reduced from 7.50 to 4.60 W/m² K.²² As a result, the fluid outlet temperature was raised by 9°C, and there was a 7% increase in thermal efficiency in comparison to the FPC system. Additionally, the lifetime of an EFPC is longer than a nonevacuated collector due to vacuum condensation and lack of humidity issues inside the collector shell.²³ Given its high thermal outputs, the EFPC works efficiently in applications such as space heating, seawater desalination, absorption chillers, meat industry, textile and leather industries, and chemical and pharmaceutical industries.¹⁵

However, there are research gaps in the design optimization of the EFPCs as well as the performance analysis for industrial hot water demand. Given that, the present research work contributes to this domain. A numerical model was developed in MATLAB, followed by prototype development for the model validation of the EFPC model. After the model validation, a parametric analysis was performed using the variables of mass flow rate, collector area, and tube spacing to determine how these parameters effect the system efficiency. Then, an economic assessment of the EFPC system was conducted for the textile industry to determine its feasibility for industrial process heat. Figure 2 provides a flowchart diagram of this research study.

2 | EFPC SYSTEM

A solar water heating system was installed at USPCAS-E, NUST Islamabad, Pakistan (33.64° N, 72.99° E). The system was comprised of two EFPCs with a total area of

FIGURE 1 Cross-section view of the evacuated flat-plate collector.

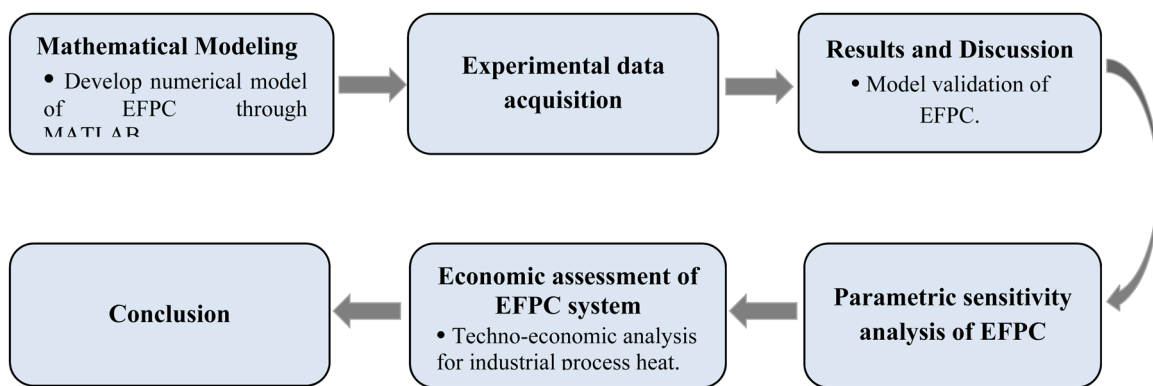
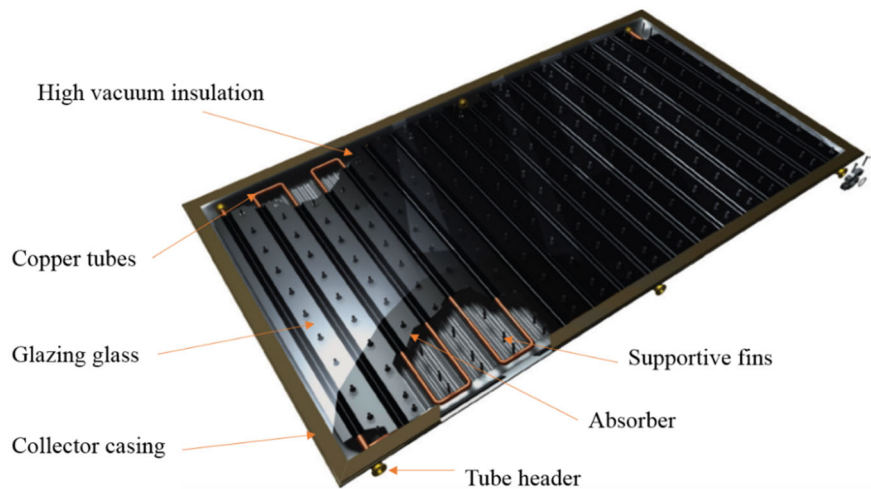


FIGURE 2 Flowchart diagram for this study. EFPC, evacuated flat-plate collector.

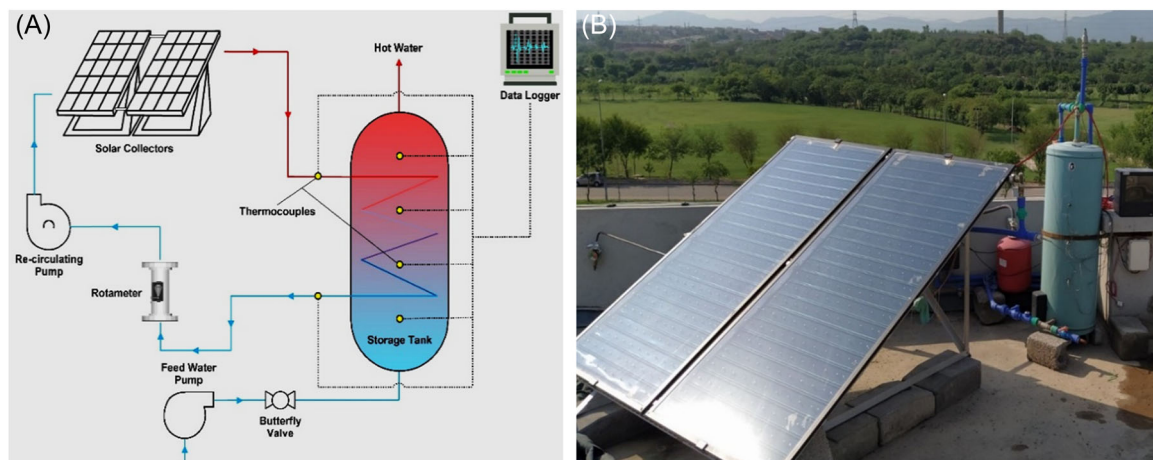


FIGURE 3 (A) Schematics of the evacuated flat-plate collector system and (B) experimental setup installed at NUST-Pakistan.

4.0 m², which was installed facing South at a 30° tilt angle, with a hybrid storage tank of 100 L capacity, a controller, Pt-1000 thermocouples, and a piping system. Figure 3 illustrates the schematics (Figure 3A) and actual setup of the EFPC solar water heating system (Figure 3B). A vacuum was created in the collector

enclosure by using a diaphragm vacuum pump to maintain a pressure of -0.8 bar inside the collector. Tubes are fixed at the bottom end of the absorber containing a heat transfer fluid (HTF) water–glycol mixture (50/50% volume), which is pumped through the solar loop using a high-efficiency circulator pump.

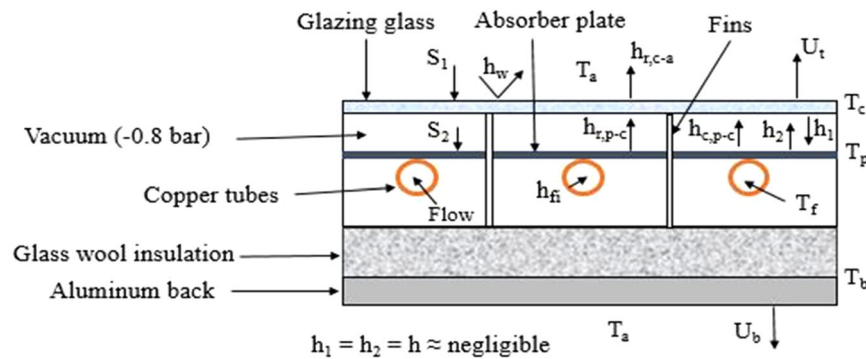


FIGURE 4 Schematic diagram of the evacuated flat-plate collector.

The fins are fixed to prevent the glazing glass from atmospheric pressure load. The bottom side of the collector is insulated with glass wool to reduce bottom losses.

There are two loops: primary and secondary. In the primary loop, the water–glycol mixture circulates with the help of a circulating pump, while the secondary loop contains water. Between the primary and secondary loops, a storage tank with a helical coil inserted inside acts as a heat exchanger (Figure 3A). For overcast days or at night a 1500-W electric heating element is connected to the storage tank, which serves as an auxiliary heater. The primary loop is filled with HTF with a filling station at a pressure of 2 bars. A pressure control valve is connected to the primary loop to maintain the pressure of HTF. The circulating pump is coupled to a pulse width modulation controller, which manages the pumping processes. The temperature and thermal loss of water and HTF are noted using thermocouples linked to the primary and secondary circuits. Thermocouples are connected to the data logger to record the temperatures. Figure 4 illustrates the cross-section view of the EFPCs. Table 1 outlines the design parameters of the collector.

3 | MATHEMATICAL MODELING

For the proposed EFPC system, the numerical model was developed in MATLAB based on the mathematical relations discussed in this section for the performance analysis. The transient analysis was conducted to examine the collector output based on parameters including solar irradiance, air temperature, wind speed, solar radiations absorbed by plate, and solar radiations absorbed by the glazing glass. The computer program developed in MATLAB is based on the algorithm shown in Figure 5.

The program begins with the collection of weather data followed by the collector specification (assuming the initial values are equal to the ambient temperature for the first section). Then, the iterative process begins, followed by calculating heat loss coefficients and heat transfer for

TABLE 1 EFPC system specifications.

Parameter	Value
Collector model	TS400 (Thermo-solar company)
Collector area	4 m ²
Absorber area	3.4 m ²
Power output per collector	1400 W
Tilt angle	30°
Storage tank capacity	100 L
Auxiliary heater	1500 W
Type of working fluid	Water–glycol mixture 50/50%
Emissivity of glazing glass	0.92
Emissivity of absorber's plate	0.95
Glazing glass transmissivity	0.90
Thickness of the glazing glass	0.004 m
Absorber's plate absorptivity	0.95
Absorber plate thickness	0.001 m
Insulation thickness	0.025 m
Absorber plate thermal conductivity	205 W/m K
Vacuum pressure	– 0.8 bar
Pressure of HTF	2 bars
Outer diameter of the tube	0.010 m
Inner diameter of the tube	0.0095 m

Abbreviations: EFPC, evacuated flat-plate collector; HTF, heat transfer fluid.

assumed temperatures. The program code is based on a matrix inversion of three matrices: $[A]$, $[T]$, and $[B]$. For new temperature values, inverted matrix $[A]^{-1}$ is used to form a new matrix $[T']$. Then, the old temperature values $[T]$ and new ones $[T']$ are compared. If the difference is greater than the convergence factor (0.01°C), then the iteration process is stopped, and the old temperature values are replaced with the new ones. In the first section, when iteration ends, the fluid outlet temperature, overall losses,

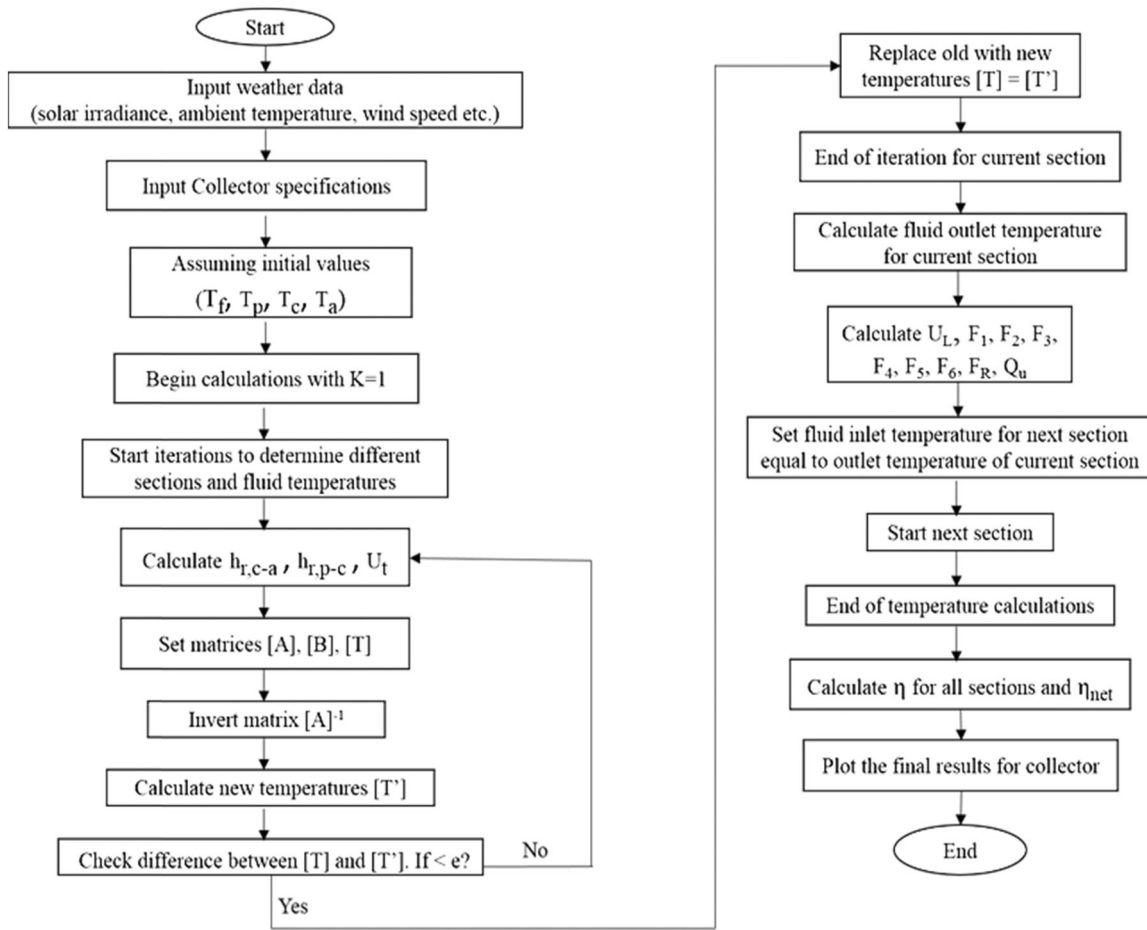


FIGURE 5 Algorithm flowchart for the MATLAB program.

heat removal factor, useful energy, and efficiencies are calculated. Then, the program sets the fluid inlet temperature for the next section equal to the fluid outlet temperature of the previous section. Following this approach, the whole collector is solved for temperatures, thermal losses, and useful energy gain.

3.1 | Thermal resistance network

Figure 6 illustrates the thermal resistance network diagram for the EFPCs. The diagram explains the temperature distribution along the flow direction with heat transfers through radiation and convection from different parts of the collector as well as overall losses in the collector. This provides the basis for numerical model development, which determines the total collector loss and efficiency.

3.2 | Energy balance

The following energy balance equations are extracted from the thermal resistance network (Figure 6) for nodal temperatures:

$$T_c : S_1 + h_{r,p-c}(T_p - T_c) + h_{nc}(T_p - T_c) = U_t(T_c - T_a), \tag{1}$$

$$T_p : S_2 = h_3(T_p - T_f) + h_{nc}(T_p - T_c) + h_{r,p-b}(T_p - T_b) + h_{r,p-c}(T_p - T_c), \tag{2}$$

$$T_f : h_3(T_p - T_f) = h_4(T_f - T_b) + Q_1, \tag{3}$$

$$T_b : h_4(T_f - T_b) + h_{r,p-b}(T_p - T_b) = U_b(T_b - T_a). \tag{4}$$

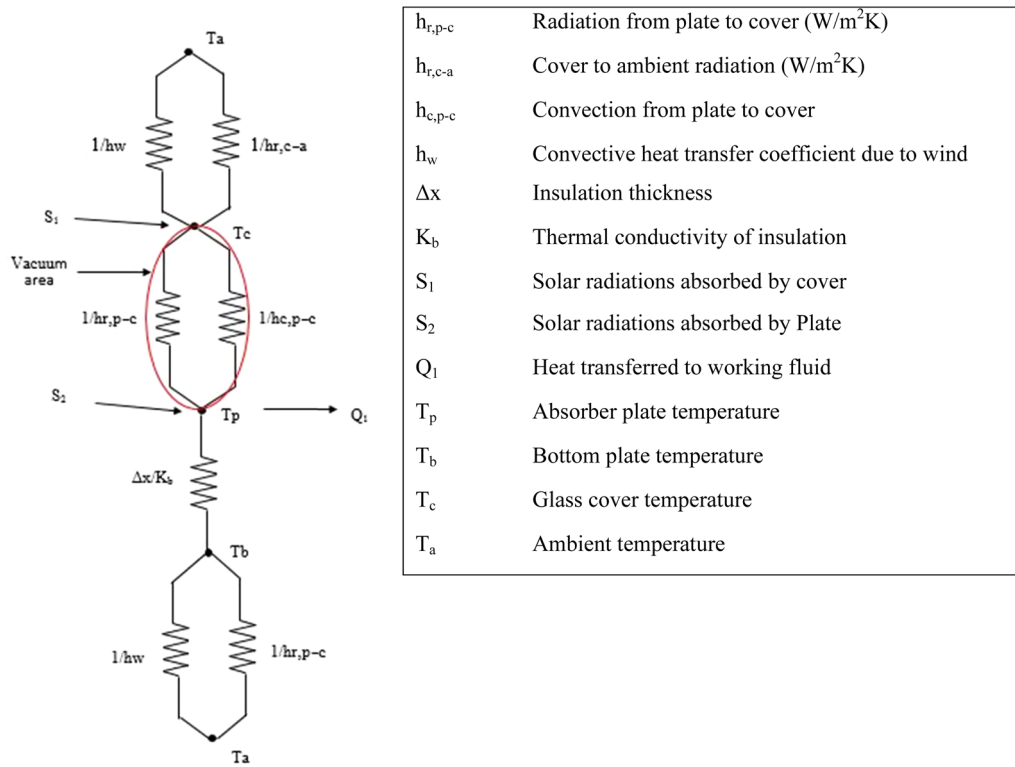


FIGURE 6 Thermal resistance network for the evacuated flat-plate collector.

3.3 | Thermal losses from the collector system

Solar radiations transmitted through glazing glass heat up the absorber and little radiations transmit back to the glazing glass. The equation for heat transfer via radiation from the absorber to glazing is expressed as²⁴

$$h_{r,p-c} = \frac{\sigma(T_p^2 + T_c^2)(T_p + T_c)}{\frac{1}{\epsilon_p} + \frac{1}{\epsilon_c} - 1} \tag{5}$$

When transmitted through the glass cover, some of the solar radiations are absorbed through the glass cover, which is transmitted to the ambient²⁴

$$h_{r,c-a} = \epsilon_c \sigma (T_c^2 + T_a^2)(T_c + T_a) \tag{6}$$

Overall, top losses from the collector depend on losses from the top glazing glass and absorber as well as the convective losses due to wind.²⁴ The convective heat transfer from the absorber to the cover becomes negligible due to the evacuated enclosure inside the collector

$$U_t = \left(\frac{1}{h_w + h_{r,c-a}} + \frac{1}{h_{c,p-c} + h_{r,p-c}} \right)^{-1} \tag{7}$$

Convective heat transfer coefficient due to wind is expressed through the following relation²⁴:

$$h_w = 5.7 + 3.8V \tag{8}$$

Convective heat transfer between the absorber and glass cover can be expressed as

$$h_{c,p-c} = Nu \frac{k_a}{L} \tag{9}$$

where K_a is the air thermal conductivity and L is the space between the absorber and glass cover. For the flow between the two plates with a tilt angle from 0° to 70° , the relation used for the Nusselt number is given as²⁴

$$Nu = 1 + 1.44 \left[1 - \frac{1708(\sin 1.8\beta)^{1.6}}{Ra \cos \beta} \right] \left[1 - \frac{1708}{Ra \cos \beta} \right]^+ + \left[\left(\frac{Ra \cos \beta}{5830} \right)^{\frac{1}{3}} - 1 \right]^+ \tag{10}$$

Raleigh number (Ra) can be found through the following relation:

$$Ra = \frac{g(T_p - T_c)L^3}{T_m \nu \alpha} \tag{11}$$

These equations are put into Equation (7) to find the total top losses (U_t). Then, the sum of the total top losses, bottom losses, and losses from the edges of the collector is the total heat loss coefficient²⁴

$$U_L = U_t + U_b + U_e. \quad (12)$$

3.4 | Heat removal factor

The heat removal factor of a collector, F_R is the ratio of the collector's real useful energy gain to the collector's actual energy gain if the surface temperature of the whole collector is the same as the inlet temperature of the fluid and heat losses are minimal. For serpentine tube arrangement, the following relation is used for the collector heat removal factor^{24,25}:

$$F_R = F_1 F_3 F_5 \left[\frac{2F_4}{F_6 \exp\left[-\frac{\sqrt{1-F_2^2}}{F_3}\right] + F_5} - 1 \right]. \quad (13)$$

F_1 , F_2 , and F_3 are dimensionless parameters and F_4 , F_5 , and F_6 are the functions of F_2 .

3.5 | Heat transfer inside the copper tubes

When solar radiation is absorbed by the plate, then energy transfers from the tube walls to the working fluid inside the tubes through convective heat transfer. The convective heat transfer coefficient within the tubes (h_{fi}) and the Nusselt number are represented by the following equations²⁴:

$$Nu = \frac{(f/8)(Re - 1000)Pr}{1.07 + 12.7 \times \sqrt{f/8} (Pr^{2/3} - 1)} \times \left(\frac{\mu}{\mu_w}\right)^n, \quad (14)$$

The heating value of n is 0.11 and 0.25 for cooling, while the Prandtl number can be calculated at fluid properties. The Darcy friction factor can be calculated through the following relation:

$$f = (0.79 \ln Re - 1.64)^{-2}, \quad (15)$$

$$Re = \frac{4\dot{m}}{\pi D_i \mu}, \quad (16)$$

$$h_{fi} = \frac{NuK}{D}. \quad (17)$$

3.6 | Collector's useful energy gain and efficiency

The engineering goal of the solar collector system is to minimize the thermal losses from the collector and to raise the useful energy yield of the thermal system. The useful energy gain for the solar collector is dependent on the heat removal factor (F_R), total thermal losses (U_L), absorbed solar radiations (S_2), and collector area (A_c)²⁴

$$Q_u = F_R A_c [S_2 - U_L(T_{fi} - T_a)]. \quad (18)$$

The collector efficiency is the ratio of solar energy collected by the fluid to the total incident solar energy in a specific time²⁴

$$n_c = \frac{Q_u}{H A_c} = \frac{F_R [S - U_L(T_{fi} - T_a)]}{H}. \quad (19)$$

4 | RESULT ANALYSIS

The numerical model based on the aforementioned relations was developed in MATLAB for transient analysis under ambient conditions. Then, the developed EFPC model is validated with the experimental results obtained from the EFPC system. A parametric analysis was performed to investigate the effect of different collector parameters on useful energy gain and collector fluid outlet temperature.

4.1 | Model validation

The simulation results were validated with experimental data for 4 days in December and January. Figure 7 presents the solar irradiance and ambient temperature trends for four different days with a maximum ambient temperature of 22°C and peak solar irradiance of 600 W/m² on January 21.

4.1.1 | Absorber and fluid outlet temperature

Figure 8 presents the results of the working fluid outlet and absorber temperature for December 23 and 24, 2020 and January 21 and 26, 2021. On December 23, 2020 (Figure 8A), the collector's absorber acquired 59.9°C of temperature from the simulation, while

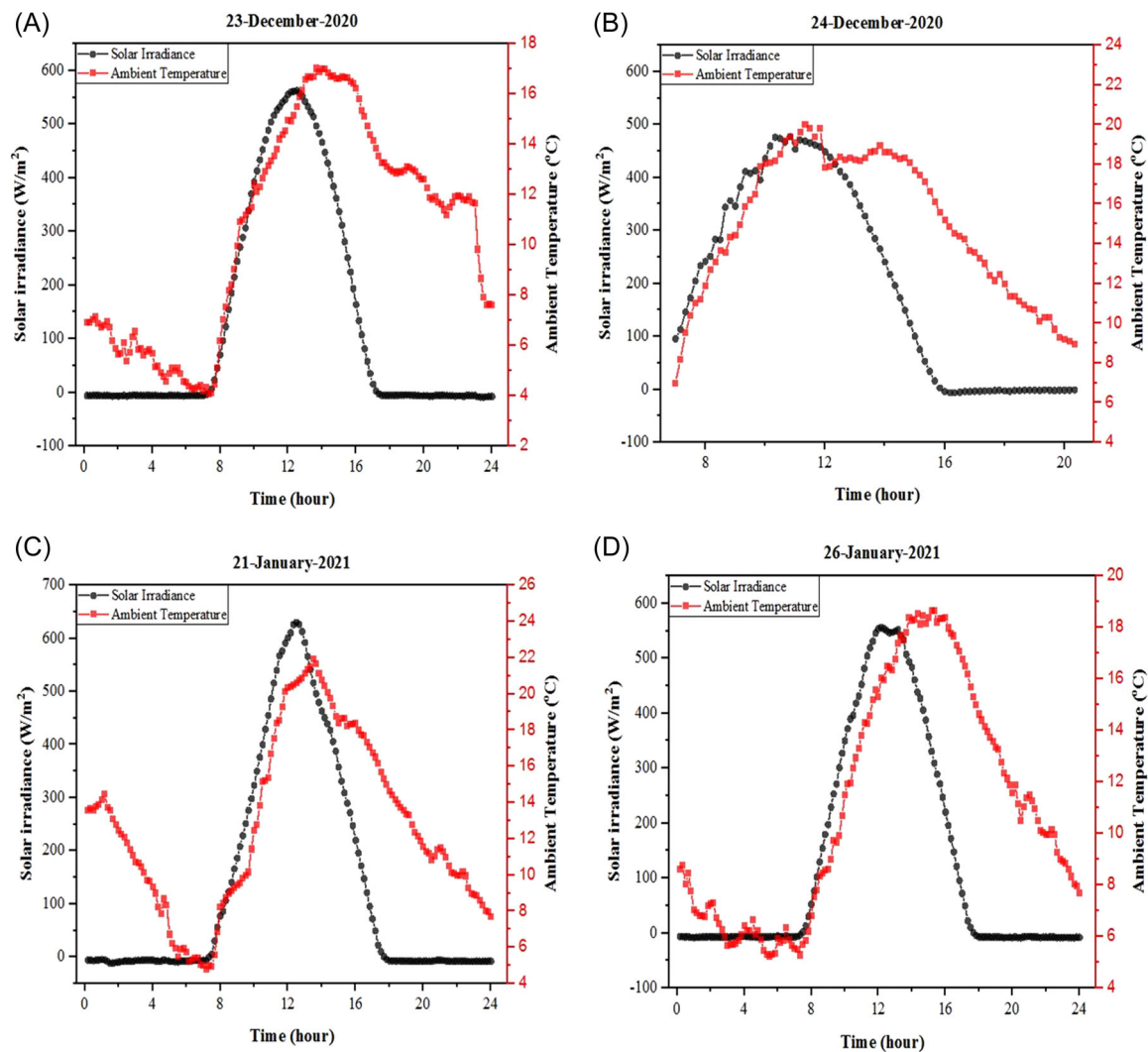


FIGURE 7 Solar irradiance and ambient temperature profiles for (A) December 23, 2020, (B) December 24, 2020, (C) January 21, 2021, and (D) January 26, 2021.

57°C was achieved from the experimental results. The absorber temperature achieves higher peaks from the vacuum inside the enclosure of the collector, which reduces convective losses from the absorber plate to the glass cover. The working fluid of the collector acquired 56.8°C of the temperature through simulation, while 55.2°C was achieved through experimental results. Both trends were concurrent with an average root mean square error (RMSE) of 2.1875 and an average percentage error of 4.2304. The linearity (R^2) value for temperature trends had an average of 0.9693. Similarly, on December 24, 2020 (Figure 8B), the absorber plate achieved a maximum temperature of 61.1°C during experimentation and had a maximum peak of 61.3°C during the simulation. The working fluid exhibited a maximum

temperature of 59.8°C through simulations and achieved a maximum temperature of 58.1°C during experimentation.

The simulation results for January 21, 2021 (Figure 8C) were compared to the experimental results, which indicated an RMSE of 2.712 on an average basis, an average percentage error of 4.914, and an R^2 of 0.9697. The model validation results for January 26, 2021 (Figure 8D) indicated an average RMSE of 2.1141, an average percentage error of 3.0235, and an R^2 of 0.9855. It is clear from Figure 8 that there is a maximum deviation of 3°C between the experimental and simulation results for the absorber and working fluid temperature. Additionally, the errors exemplify how the validation results support the EFPC model.

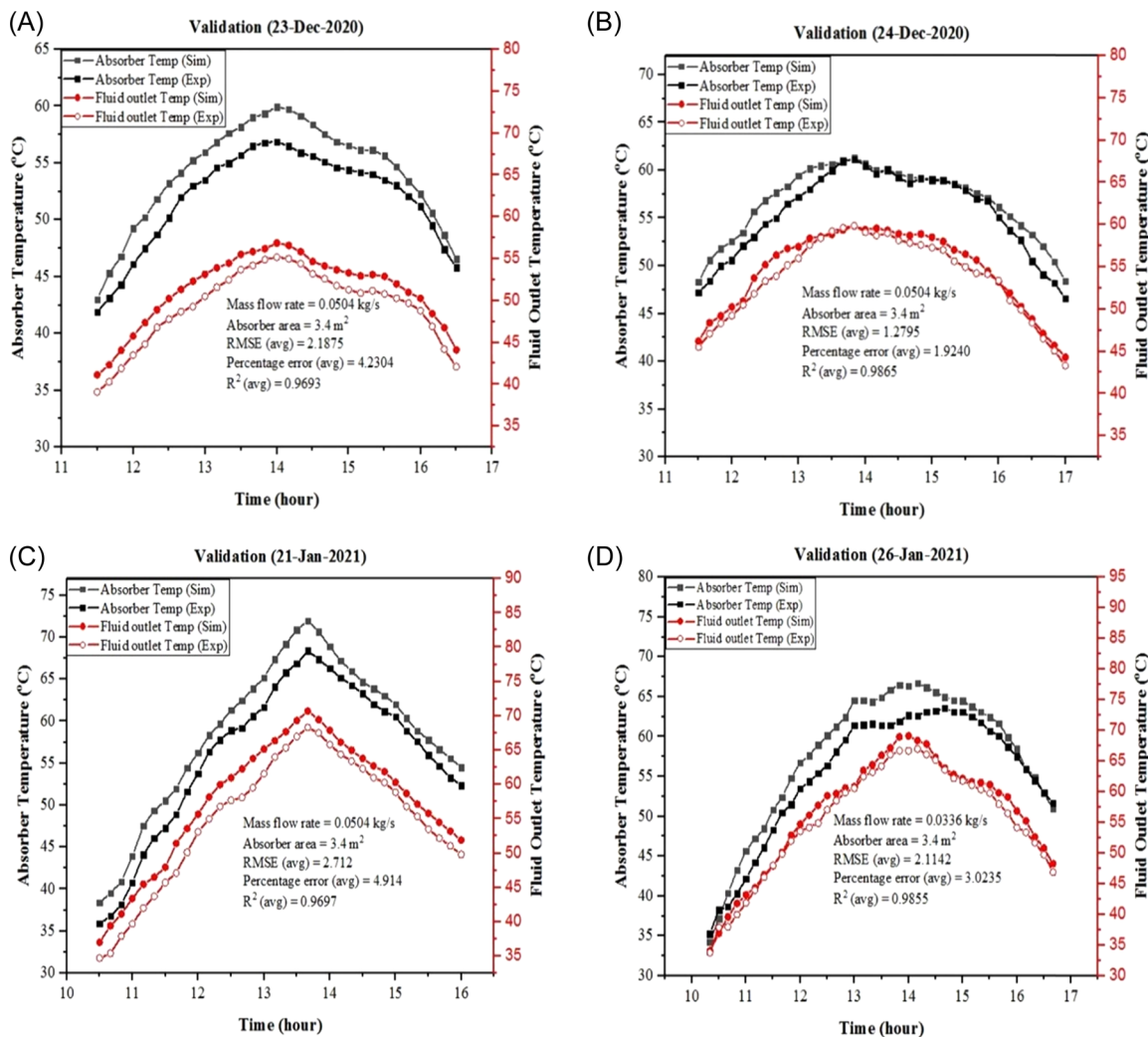


FIGURE 8 Model validation of fluid outlet and absorber temperature for (A) December 23, 2020, (B) December 24, 2020, (C) January 21, 2021, and (D) January 26, 2021. RMSE, root mean square error.

4.1.2 | Thermal efficiency

The EFPC model validated the thermal efficiency under climatic conditions on December 23 and 24, 2020 as shown in Figure 9. The thermal efficiency observed on December 23 from the simulation was 0.8053, and a maximum of 0.7847 was achieved during the experiment. On December 24, model simulations exhibited an efficiency of 0.8263 and a maximum efficiency of 0.8155 for the experimental results. The results showed an average RMSE of 0.0244, an average percentage error of 4.03, and an average R² for a polynomial of 0.9877. The RMSE and percentage error indicate that the developed EFPCs are consistent with the actual system. Table 2 presents the RMSE, percentage errors, and R² taken from the experimental validation of the EFPCs.

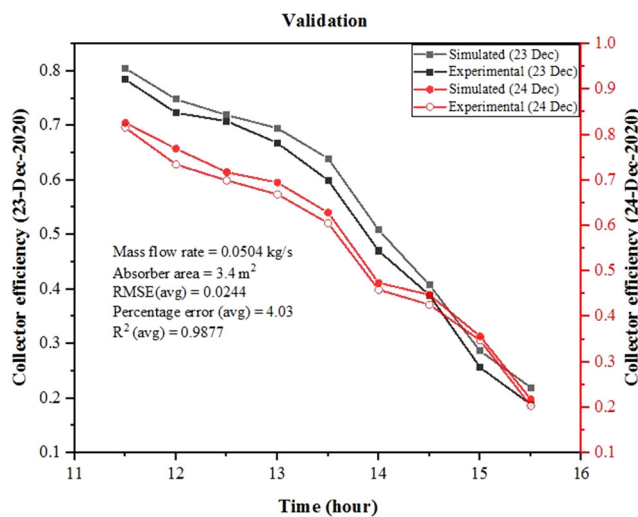


FIGURE 9 Model validation for collector efficiency. RMSE, root mean square error.

TABLE 2 Summary of model validation results.

Date	Parameter	RMSE	Percentage error (avg)	R^2 (avg)
Dec 23, 2020	Absorber temperature	2.3511	3.9310	0.9693
	Fluid outlet temperature	1.5849	2.6197	0.9784
Dec 24, 2020	Absorber temperature	1.5085	2.2761	0.9865
	Fluid outlet temperature	1.0505	1.5720	0.9789
Jan 21, 2021	Absorber temperature	2.2242	3.6788	0.9644
	Fluid outlet temperature	2.7177	4.1448	0.9659
Jan 26, 2021	Absorber temperature	2.8157	3.9090	0.9945
	Fluid outlet temperature	1.4127	2.1380	0.9765
Dec 23, 2020	Thermal efficiency of the collector	0.0282	6.6223	0.9870
Dec 24, 2020		0.0207	3.8457	0.9835

Abbreviation: RMSE, root mean square error.

5 | EFFECT OF DESIGN PARAMETERS ON SYSTEM PERFORMANCE

This section examines how changing the collector design conditions and parameters effect the collector efficiency, useful energy gain, and fluid outlet temperature. The developed model was simulated with a variable collector area, mass flow rate, and tube spacing to obtain the output results of the collector model on January 26, 2021. Moreover, different ratio of the water–glycol mixture is investigated for the thermal conductivity of the fluid and its effect on useful energy gain.

5.1 | Collector absorber area and useful energy gain

Figure 10 shows the results of the effect of the absorber area on useful energy gain, which indicated an average increase of 310 W per unit in the collector area. Increasing the absorber area enhances the useful energy gain of the collector as per Equation (18).^{19,26} Based on the results, the absorber area is considered an important parameter of the collector.

5.2 | Collector absorber area and working fluid outlet temperature

Figure 11 examines the influence of the collector's absorber area on the working fluid outlet temperature. The diagram shows how collectors with a maximum absorber area obtain higher peaks of fluid outlet temperatures, while the working fluid temperature is lower for smaller absorber areas. By

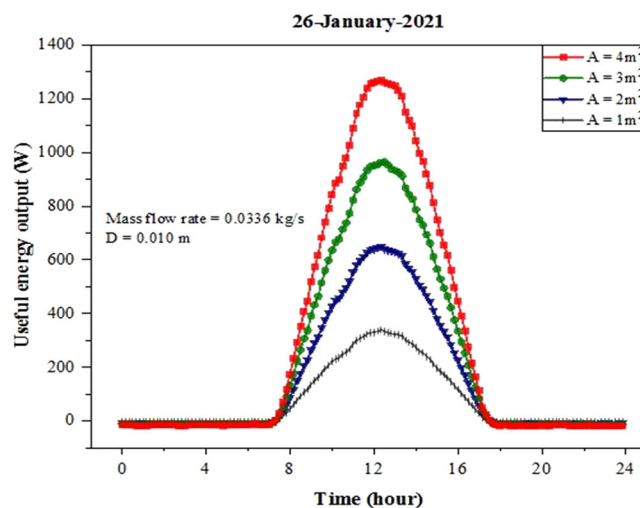


FIGURE 10 Effect of absorber area on useful energy gain.

increasing the absorber area, the surface exposed to solar radiation correspondingly increases, thus absorbing greater solar radiation. This in turn raises the heat gain of the water–glycol mixture in the copper tubes. However, a larger collector area also results in greater thermal losses as the surface is exposed to ambient increases, thus decreasing thermal efficiency. As such, during the design process for the EFPCs, the impact of the collector area on thermal losses and efficiency should be taken into consideration.

5.3 | Mass flow rate and working fluid outlet temperature

Figure 12 depicts the influence of the mass flow rate through the collector on the working fluid outlet temperature. The model was computed with mass

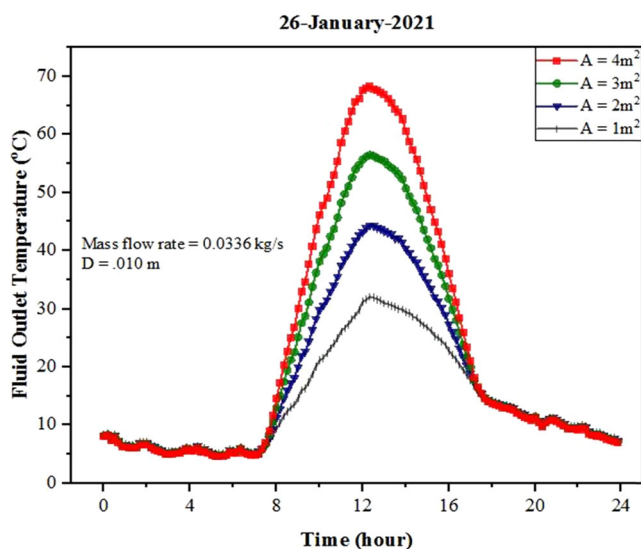


FIGURE 11 Impact of absorber area on fluid outlet temperature.

flow rates of 0.0252, 0.028, 0.0308, and 0.0336 kg/s. The working fluid temperature at the collector outlet is higher at minimum flow rates and then decreases when the working fluid flow rate increases. The temperature drops because the fluid has less retention time to absorb heat inside the heating loop as the mass flow rate of the fluid increases. The mass flow rate of the working fluid is a critical parameter for attaining the desired outputs of the thermal collector.

5.4 | Tube spacing and the useful energy gain of the collector

Figure 13 illustrates the impact of tube spacing on the useful energy gain of the collector. Simulations were performed with variable tube spacing of 0.050, 0.070, 0.090, and 0.110 m to examine its impact on energy output. Figure 13 demonstrates that when the collector has minimum tube spacing, higher thermal energy outputs are attained, whereas maximum tube spacing achieves lower peaks of thermal energy. Additionally, the diagram depicts how every 0.020 m increase in tube spacing leads to an average of 55 W reduction in the useful energy gain of the collector.

However, by increasing the tube spacing the absorber area between the two tubes loses more heat to the bottom collector, which results in lower useful energy. Conversely, smaller tube spacing exposes less area for bottom losses, thus leading to higher useful energy.

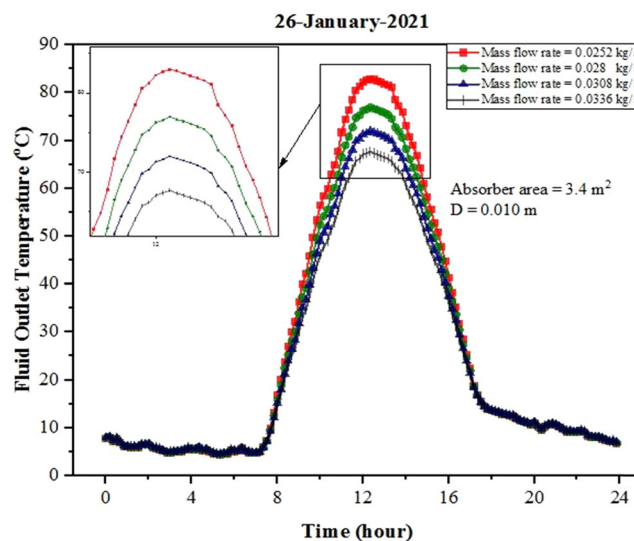


FIGURE 12 Impact of variable mass flow rate on fluid outlet temperature.

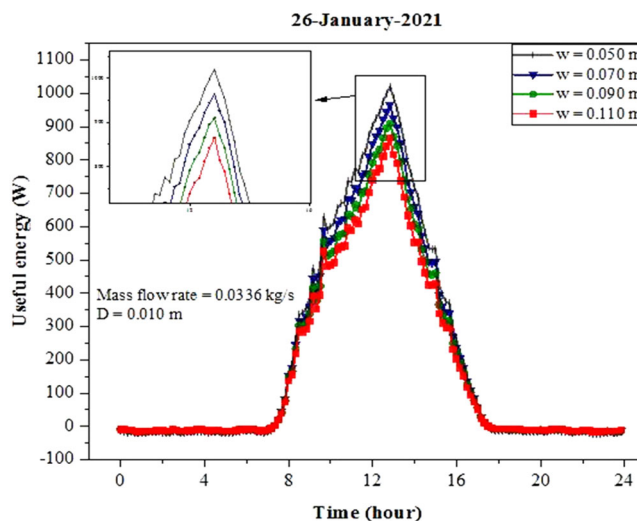


FIGURE 13 Influence of collector's tube spacing on useful energy gain.

5.5 | Water-glycol mixture ratios and its effect on useful energy gain

The goal of this comparative study is to determine the effect of different HTF mixtures on useful energy gain. The thermal conductivity of different water-glycol mixtures is taken at 80°C.²⁷ For each 25% addition of glycol in the working fluid, the useful energy gain was raised by 90–110 W. The useful energy gain of the systems will be higher for the working fluids having low thermal conductivities. Moreover, by increasing the proportion of glycol in the mixture increases the viscosity of HTF, which effects the useful energy gain. However,

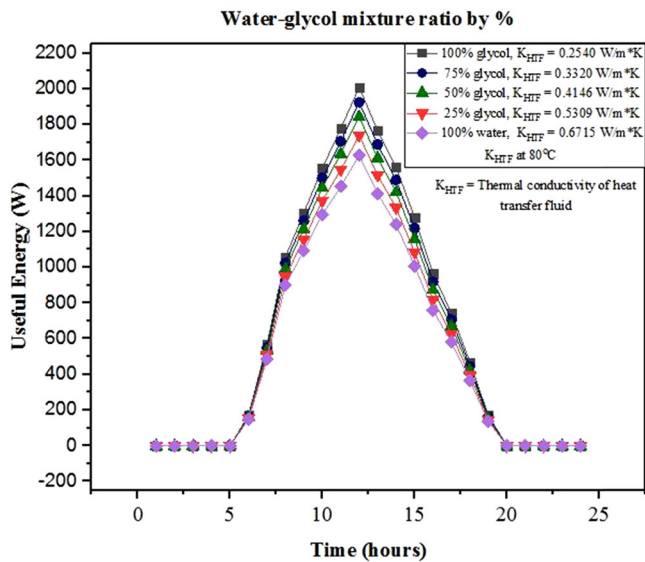


FIGURE 14 Change in useful energy gain against different heat transfer fluid mixtures.

higher viscous fluids consume higher pumping power. So, the viscosity effect should be considered while selecting the HTF mixture.

Figure 14 shows the change in useful energy gain with varying the glycol concentrations in a water–glycol mixture.

6 | ECONOMIC ANALYSIS OF EFPC WATER HEATING SYSTEM FOR INDUSTRIAL PROCESS HEAT: A CASE STUDY

The EFPC solar water heating system can be utilized for a multitude of purposes, including domestic and industrial applications. Within the textile industry, processes such as washing, heating, bleaching, dyeing, weaving, and wet processing use hot water and steam generated with conventional boilers. These processes account for a huge share of the industrial process heat demand, which creates the potential for use of solar water heating systems.

6.1 | Energy consumption in a textile industry

In the textile industry, a unit that produces 9000 kg/day of fabric, on average, will consume 36,000 L of water per day.²⁸ An economic analysis was conducted on the data collected from a textile industry located in Faisalabad,

TABLE 3 Average energy consumption profile of the textile industry for process heat.

Parameter	Value
Boiler type	Fire tube boiler
Fuel used	Natural gas
Capacity of boiler	5 ton/h
Inlet temperature of boiler	90°C
Boiler efficiency	0.85
Water consumption in the textile industry per day	36 ton
Total water consumption from 9 a.m. to 4 p.m.	10.5 ton
Steam temperature at boiler outlet	156–162°C
Feed water tank inlet temperature (summer)	30°C
Feed water tank inlet temperature (winter)	20°C
Feed water tank outlet temperature	90°C
Boiler pressure	6 bar
Natural gas consumption for rising temperatures up to 90°C during summer (9 a.m.–4 p.m.)	71.82 m ³
Natural gas consumption for rising temperatures up to 90°C during winter (9 a.m.–4 p.m.)	83.79 m ³

Pakistan. Table 3 presents the consumption profile of the textile industry for process heat.

6.2 | EFPC solar water heating system for industrial process heat

In the industrial facility under study, the inlet temperature of water in the feed water tank is 30°C in the summer and 20°C in the winter. Using natural gas, the feed water temperature rises to 90°C. Then, water is supplied to the boiler for steam generation, which creates super-saturated steam at 180°C. To diminish the need for natural gas, the solar water heating system is proposed to supply hot water to the feed tank during sunlight hours (9 a.m.–4 p.m.).

In an industrial facility, condensate water (35%–40%) from the condensate tank returns to the boiler at a temperature of 85–90°C and flash steam is utilized within the facility of the processing unit. The loss in mass flow of condensate water and flash steam is due to the direct steam heating and steam leakages

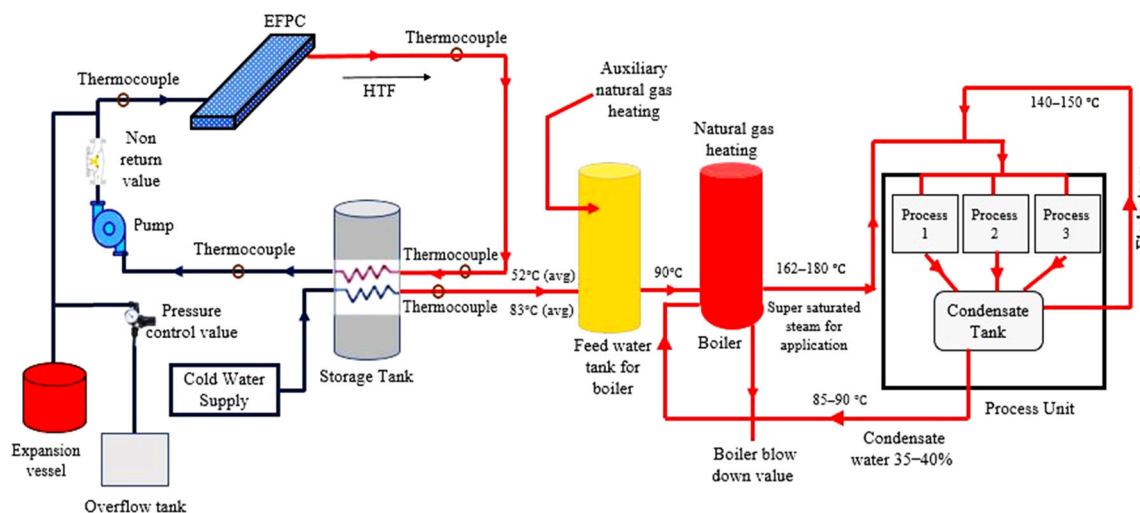


FIGURE 15 Schematic diagram of the evacuated flat-plate collector (EFPC) system integrated with the industrial process heating system. HTF, heat transfer fluid.

in old machines. Moreover, the total demand for hot water is 60,000 L/day. Condensate return covers up to 24,000 L/day about 40% of the total demand. The remaining 36,000 L/day should be provided through a feed water tank, of which 10,500 L will be heated through the current solar thermal collector system in the sunshine hours. Figure 15 shows the proposed EFPC system integrated with an industrial process heating system.

Table 4 outlines the specifications for the solar water heating system design to achieve the required temperature and mass flow rate for process heat in the textile industry. The EFPC model was developed in MATLAB and the average temperatures for summer (June) and winter (February) for the year 2021 were calculated. Based on the design conditions, the average temperature achieved between 9 a.m. and 4 p.m. at the storage tank outlet was 83°C in June and 52°C in February. As shown in Figure 15, filling the temperature gaps between 83–90°C and 52–90°C is achieved through auxiliary natural gas heating in the feed water tank, which is then supplied to the boiler. Before integrating the EFPC system, the consumption and cost of natural gas to achieve outlet temperatures of 83°C in the summer and 52°C in the winter would have been significant. However, savings are generated when hot water is supplied through the EFPC system to the feed water tank. Table 5 outlines the results for natural gas savings and Table 6 provides the cost of natural gas savings achieved with the use of solar water heating and the capital cost of the EFPC system.

Solar fraction is the ratio of the total energy supplied by the solar heating system to the total energy required.

TABLE 4 Design specifications of the EFPC system for process heat in the textile industry.

Parameter	Value
Total number of collectors	21
Total area of the collectors	42 m ²
Total absorber area	36 m ²
Working fluid	Water–glycol mixture
Mass flow rate	0.42 kg/s
Storage tank outlet temperature average (June)	83°C
Storage tank outlet temperature average (February)	52°C
Time duration	9 a.m.–4 p.m.

Abbreviation: EFPC, evacuated flat-plate collector.

The solar fraction for any system can be determined by the following relation²⁴:

$$SF = \frac{\text{Solar Energy supplied}}{\text{Total Energy required}} \quad (20)$$

Figure 16 shows the solar fraction for the EFPC system, which highlights an 88% (average) solar fraction during the summer and 45% (average) during the winter. The remaining 12% in summer and 55% in winter is fulfilled through auxiliary natural gas heating. Figure 17 illustrates the payback period for the capital cost for the EFPC system for textile industrial process heat.

The economic feasibility of the EFPC system has been compared to solar water heating based on ETCs and FPCs (Table 7). In comparison to FPCs and ETCs, the

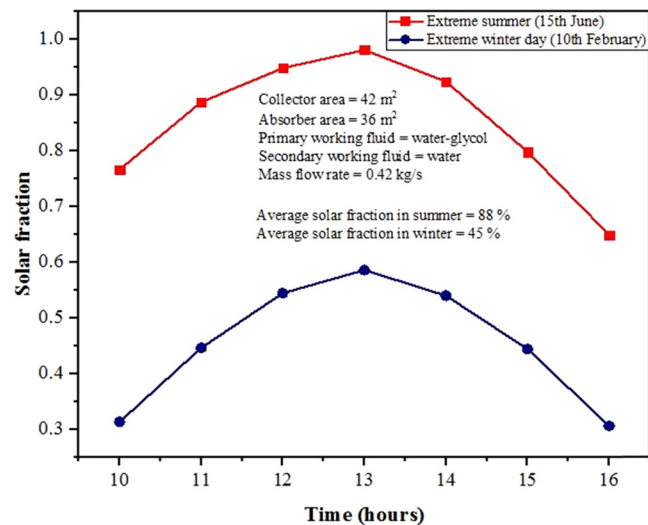
TABLE 5 Calculation results for natural gas savings to rise temperature of water with EFPCs.

Parameter	Value
Energy required to rise 1°C temperature of 1 ton of water	4.18 MJ
Energy in 1 m ³ of natural gas in MMBTU	0.0408 MMBTU
Energy in 1 m ³ of natural gas in joules	43.06 MJ
Total energy in 1 m ³ of natural gas for respected boiler	36.6 MJ
Natural gas required for 1 ton of water to rise 1°C temperature	0.114 m ³
Natural gas required for 1°C rise of 10.5 ton of water	1.197 m ³
Natural gas savings in summer for 53°C units (30–83°C) temperature rise (on an average basis)	63.441 m ³
Natural gas savings in winter for 32°C units (20–52°C) temperature rise (on an average basis)	38.30 m ³

Abbreviation: EFPC, evacuated flat-plate collector.

TABLE 6 Table 6. Cost of natural gas savings and capital cost of the collector model.

Parameter	Cost in US\$
Cost of natural gas per m ³	0.31
Natural gas saving for 6 months (summer)	3540
Natural gas saving for 6 months (winter)	2137.4
Total savings per year	5677
Cost per m ² area of the collector	1001.5
Capital cost for 42 m ² area of the collector	42,063
Payback period	7.4 years


FIGURE 16 Solar fraction for the evacuated flat-plate collector system.

results indicate that the EFPC system can be an economical and sustainable energy system to fulfil the industrial process heat demand with a lower payback period.

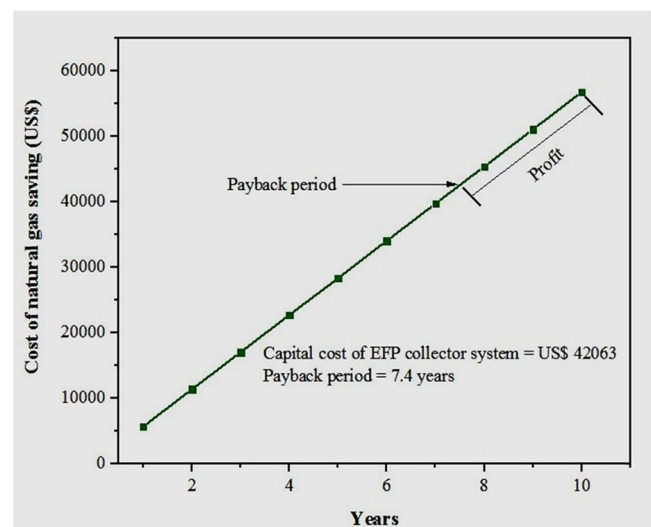

FIGURE 17 Payback period of the evacuated flat-plate (EFP) collector solar water heating system designed for the textile industry.

TABLE 7 Financial comparison of solar collectors for industrial process heat.

Solar collector	Reference	Payback period (years)
FPC	29	12.6
ETC	30	9
EFPC	Current study	7.4

Abbreviations: EFPC, evacuated flat-plate collector; ETC, evacuated tube collector; FPC, flat-plate collector.

7 | CONCLUSION

This study analyzed the performance of a solar water heating system based on an EFPC. This novel solar harvesting technology was investigated for its application in industrial process heat demand. The numerical model of the EFPC developed in MATLAB was based on the

thermal energy balance, and considered the useful energy gain, heat removal factor, and thermal efficiency of the collector. The developed program code was simulated using the design conditions of the proposed EFPC solar water heating system and validated with experimental results.

The model validations exhibited the highest RMSE of 2.758 and the highest percentage error of 5.084 for the fluid outlet temperature on January 21, 2021, which substantiates the accuracy of the model. The results showed:

- A maximum fluid outlet temperature of 98°C in June and 69°C in January, and the maximum useful energy observed in January was 1300 W. The maximum observed thermal energy was 78%, and the thermal collector with vacuum had an efficiency of 69%.
- Due to the evacuated collector enclosure, convective losses from the absorber plate to the glass cover were negligible, which substantially lowered the coefficient thermal losses from 7.50 to 4.60 W/m² K. This ultimately resulted in greater thermal outputs.

The influence of variable collector area, mass flow rate, spacing between the tubes, and different ratios of water–glycol mixture on the collector outputs was investigated in the MATLAB model. The parametric analysis revealed:

- Increasing the collector area will result in an increase in useful energy gain and working fluid outlet temperature.
- Increasing the mass flow rate of the working fluid will decrease the outlet temperature of the working fluid.
- The smaller the tube spacing the greater the useful energy gains by the EFPCs.
- Higher the percentage of glycol in the mixture greater will be the useful energy gain.

The economic analysis of the proposed EFPC solar water heating system was conducted for a hot water supply in a textile industry in Pakistan. The results indicated a payback period of 7.4 years for the capital costs of the collector system. As such, this analysis highlighted how a solar water heating system based on an EFPC is sustainable and economically feasible for industrial process heat demands. Additionally, this research provides policymakers and investors with relevant information regarding the beneficial use of solar heating systems.

NOMENCLATURE

C_b	bond conductance
e	convergence factor

f	Darcy friction factor
F_i	dimensionless parameters ($i = 1, 2, 3, \dots, 6$)
F_R	heat removal factor
$h_{1,2,3,4}$	heat transfer due to forced convection
$h_{c,p-c}$	convection from plate to cover (W/m ² K)
h_{fi}	convective heat transfer inside the tubes
h_{nc}	heat transfer due to natural convection
$h_{r,c-a}$	cover to ambient radiation (W/m ² K)
$h_{r,p-b}$	radiation from absorber to bottom plate
$h_{r,p-c}$	from plate to cover (W/m ² K)
h_w	convective heat transfer due to wind
H	solar irradiance (W/m ²)
k	plate conductivity
K_b	insulation thermal conductivity
\dot{m}	mass flow rate of working fluid (kg/s)
Nu	Nusselt number
Pr	Prandtl number
R^2	linearity of the graph
Ra	Raleigh number
Re	Reynold number
S_1	solar radiations absorbed by cover
S_2	solar radiations absorbed by absorber
T_a	ambient temperature (°C)
T_b	bottom plate temperature
T_c	glass cover temperature (°C)
$T_{f_{out}}$	fluid outlet temperature (°C)
T_p	absorber plate temperature (°C)
U_b	bottom losses
U_e	edge losses of the collector
U_L	overall losses
U_t	total top losses
V	wind speed
W	tube spacing
α	absorptivity
β	tilt angle
δ	thickness of the plate
Δx	thickness of insulation
ε_c	emissivity of the glass cover
ε_p	emissivity of absorber plate
μ	dynamic viscosity
ν	kinematic viscosity
σ	Stefan–Boltzmann constant
τ	transmissivity


ACKNOWLEDGMENTS


The authors would like to thank US-Pakistan Center for Advanced Studies in Energy at the National University of Sciences and Technology (NUST), Islamabad, Pakistan and the Graduate School of Economics and Management, Ural Federal University, and the Russian Federation for their support to conduct this research work. Open access funding provided by the Qatar National Library.

CONFLICT OF INTEREST STATEMENT

The authors declare no conflict of interest.

ORCID

Muhammad Mujtaba Abbas  <http://orcid.org/0000-0001-9134-9002>

Fares Almomani  <http://orcid.org/0000-0003-4785-4567>

REFERENCES

- Almomani F, Al Ketife A, Judd S, Shurair M, Bhosale RR, Znad H, Tawalbeh M. Impact of CO₂ concentration and ambient conditions on microalgal growth and nutrient removal from wastewater by a photobioreactor. *Sci Total Environ.* 2019;662:662-671. doi:10.1016/j.scitotenv.2019.01.144
- Abdelsalam E, Almomani F, Ibrahim S. A novel hybrid solar chimney power plant: performance analysis and deployment feasibility. *Energy Sci Eng.* 2022;10:3559-3579. doi:10.1002/ese3.1240
- Sovacool BK, Griffiths S, Kim J, Bazilian M. Climate change and industrial F-gases: a critical and systematic review of developments, sociotechnical systems and policy options for reducing synthetic greenhouse gas emissions. *Renew Sustain Energy Rev.* 2021;141:110759. doi:10.1016/j.rser.2021.110759
- Zheng X, Streimikiene D, Balezentis T, Mardani A, Cavallaro F, Liao H. A review of greenhouse gas emission profiles, dynamics, and climate change mitigation efforts across the key climate change players. *J Clean Prod.* 2019;234:1113-1133. doi:10.1016/j.jclepro.2019.06.140
- Judd SJ, Al Momani FAO, Znad H, Al Ketife AMD. The cost benefit of algal technology for combined CO₂ mitigation and nutrient abatement. *Renew Sustain Energy Rev.* 2017;71:379-387. doi:10.1016/j.rser.2016.12.068
- Maaz Mufti G, Jamil M, Nawaz M, Mobeen-ur-Rehman, Zulqadar Hassan S, Kamal T. Evaluating the issues and challenges in context of the energy crisis of Pakistan. *Indian J Scie Technol.* 2016;9(36):1-7. doi:10.17485/ijst/2016/v9i36/102146
- Raza MY, Wasim M, Sarwar MS. Development of renewable energy technologies in rural areas of Pakistan. *Energy Source Part A.* 2020;42(6):740-760. doi:10.1080/15567036.2019.1588428
- Achard FC. Pakistan economic survey 2021–2022. In: Achard FC, Kirsten C, Zeisler K, eds. *Ausführliche Beschreibung der Methode, nach welcher bei der Kultur der Runkelrübe verfahren werden muß, um ihren Zuckerstoff nach Möglichkeit zu vermehren.* De Gruyter; 2022:32-33. doi:10.1515/9783112593806-014
- Shah SAA, Solangi YA. A sustainable solution for electricity crisis in Pakistan: opportunities, barriers, and policy implications for 100% renewable energy. *Environ Sci Pollut Res.* 2019;26(29):29687-29703. doi:10.1007/s11356-019-06102-0
- Almaita E, Abdelsalam E, Al Nawafah H, AlShkoor S, Almomani F. Analysis and feasibility of integrating a new and novel hybrid solar chimney power plant with a traditional electrical grid. *Int J Energy Res.* 2022;46(7):9194-9205. doi:10.1002/er.7795
- Kamran M. Current status and future success of renewable energy in Pakistan. *Renew Sustain Energy Rev.* 2018;82609-617. doi:10.1016/j.rser.2017.09.049
- Farooq M, Shakoor A. Severe energy crises and solar thermal energy as a viable option for Pakistan. *J Renew Sustain Energy.* 2013;5(1):013104. doi:10.1063/1.4772637
- Freeman J, Hellgardt K, Markides CN. An assessment of solar-thermal collector designs for small-scale combined heating and power applications in the United Kingdom. *Heat Transfer Eng.* 2015;36(14-15):1332-1347. doi:10.1080/01457632.2015.995037
- Farjana SH, Huda N, Mahmud MAP, Saidur R. Solar process heat in industrial systems—a global review. *Renew Sustain Energy Rev.* 2018;822270-2286. doi:10.1016/j.rser.2017.08.065
- Sharma AK, Sharma C, Mullick SC, Kandpal TC. Solar industrial process heating: a review. *Renew Sustain Energy Rev.* 2017;78124-137. doi:10.1016/j.rser.2017.04.079
- Çiftçiöğlü GA, Kadırgan MAN, Kadırgan F. High efficiency solar thermal collectors utilization in process heat: a case study of textile finishing industry. *World Acad Eng.* 2017;11(3):350-353.
- Gao D, Gao G, Cao J, et al. Experimental and numerical analysis of an efficiently optimized evacuated flat plate solar collector under medium temperature. *Appl Energy.* 2020;269:115129. doi:10.1016/j.apenergy.2020.115129
- Moss RW, Henshall P, Arya F, Shire GSF, Eames PC, Hyde T. Simulator testing of evacuated flat plate solar collectors for industrial heat and building integration. *Sol Energy.* 2018;164:109-118. doi:10.1016/j.solener.2018.02.004
- Moss RW, Henshall P, Arya F, Shire GSF, Hyde T, Eames PC. Performance and operational effectiveness of evacuated flat plate solar collectors compared with conventional thermal, PVT and PV panels. *Appl Energy.* 2018;216:588-601. doi:10.1016/j.apenergy.2018.01.001
- Moss R, Shire S, Henshall P, Arya F, Eames P, Hyde T. Performance of evacuated flat plate solar thermal collectors. *Therm Sci Eng Progr.* 2018;8:296-306. doi:10.1016/j.tsep.2018.09.003
- Alam M, Singh H, Suresh S, Redpath DAG. Energy and economic analysis of vacuum insulation panels (VIPs) used in non-domestic buildings. *Appl Energy.* 2017;188:1-8. doi:10.1016/j.apenergy.2016.11.115
- Hassan Z, Mahmood M, Waqas A, Ali M, Ahmed N. Mathematical Modeling and Thermal Analysis of Evacuated Flat Plate Collector in Pakistan: 2021 International Conference on Emerging Power Technologies (ICEPT), Topi, Pakistan, 31 May 2021. IEEE; 2021. doi:10.1109/ICEPT51706.2021.9435492.
- Beikircher T. Process steam production. *Sol Energy.* 1999;65(2):111-118.
- Duffie JA, Beckman WA, McGowan J. Solar engineering of thermal processes. *Am J Phys.* 1985;53(4):382. doi:10.1119/1.14178
- Klevinskis A, Bučinskas V. Analysis of a flat-plate solar collector/Plokščiojo Saulės Kolektoriaus Tyrimas. *Moksl Liet Ateitis.* 2012;3(6):39-43. doi:10.3846/mla.2011.108
- Duvuna GA, Tashiwa YI, Zhigilla YI. Parametric study of an active solar flat-plate collector water heater. *Niger J Technol.* 2019;38(4):876. doi:10.4314/njt.v38i4.9

27. Obermeier E, Fischer S, Bohne D. Thermal conductivity, density, viscosity, and Prandtl numbers of di- and triethylene glycol–water mixtures. *Ber Bunsenges Phys Chem*. 1985;89(7): 805-809. doi:10.1002/bbpc.19850890716
28. Samanta KK, Pandit P, Samanta P, Basak S. 3—*Water Consumption in Textile Processing and Sustainable Approaches For its Conservation*. Elsevier; 2019.
29. Nauroz Ali E, Liaquat R, Ali M, Waqas A, Shahzad N. Techno-economic and GHG mitigation analyses based on regional and seasonal variations of non-concentrating solar thermal collectors in textile sector of Pakistan. *Renew Energy Focus*. 2022;42:165-177. doi:10.1016/j.ref.2022.06.005
30. Hussain MA, Rashid M, Khan S, Rahim A. A techno-economic analysis of solar thermal water heaters in Pakistan. *Sukkur IBA J Emerg Technol*. 2019;2(2):36-45. doi:10.30537/sjet.v2i2.457

How to cite this article: Hassan Z, Mahmood M, Ahmed N, et al. Techno-economic assessment of evacuated flat-plate solar collector system for industrial process heat. *Energy Sci Eng*. 2023;11:2185-2201. doi:10.1002/ese3.1447